PRELIMINARY RESULTS OF THE *MARINER IV* OCCULTATION MEASUREMENT OF THE ATMOSPHERE OF MARS

A. J. Kliore, D. L. Cain, and G. S. Levy
Jet Propulsion Laboratory
Pasadena, California

V. R. Eshleman and G. Fjeldbo
Stanford University
Stanford, California

F. D. Drake
Cornell University
Ithaca, New York

I. Introduction

This paper is intended as a review of the preliminary results of the radio occultation measurement of the atmosphere of Mars that was carried out as the *Mariner IV* spacecraft passed behind the planet on July 15, 1965. Most of these results are abstracted from previous publications (Ref. 1).

From the very precise data that were acquired in the course of the experiment, preliminary analysis has produced several unexpected results. Among these the following points summarize the findings.

1. The values of density, pressure, scale height, and temperature near the surface of Mars have been found to be lower than expected.
2. Based on the occultation results, as well as terrestrial spectroscopic measurements of CO_2 abundance in the atmosphere of Mars, it is concluded that carbon dioxide must be the primary constituent.

II. Experiment

The *Mariner IV* Occultation Experiment (Ref. 2) has been carried out by investigators from the Jet Propulsion Laboratory, Stanford University, and Cornell University. Previous knowledge of such atmospheric properties as the surface pressure and density, as well as scale height, has been quite poorly defined. The surface pressure, as deduced from recent spectroscopic observations of weak and strong CO_2 absorption bands, was thought to lie

somewhere between 10 and 40 mb (Refs. 3, 4). The vertical structure of the atmosphere has not previously been accessible to direct Earth-based measurement, and could only be estimated by assuming atmospheric constituents and temperatures.

The results of the *Mariner IV* occultation experiment, when fully analyzed, will provide an improved definition of the surface density and pressure, as well as the vertical structure of the atmosphere and the electron density profile of the ionosphere of Mars. However, even a rather superficial analysis performed in the time since acquisition of the data on July 15 has yielded significant results.

As the spacecraft approached the limb of the planet, the presence of an atmosphere and ionosphere caused the velocity of propagation of the radio signal to deviate from that in free space because of the non-unity index of refraction of the neutral and ionized media. Also, the radial gradient of the effective index of refraction caused the radio beam to be refracted from a straight line path. Both of these effects caused the phase path length of the propagation to differ from what would have been observed in the absence of an atmosphere and ionosphere. Thus, since the geometry, obtained from the estimated trajectory, is known, the measured deviation in phase can be used to estimate the spatial characteristics of the index of refraction (or refractivity) in the atmosphere and ionosphere by a process of integral inversion or by model fitting (Refs. 5–7).

The analysis of doppler tracking data taken before and after planetary encounter yields the trajectory of the spacecraft at the time of occultation with such precision that the range rate of the spacecraft is known to an accuracy of 0.0015 m/sec. Thus any significant deviation of the received doppler data from orbit determination predictions can be expected to be caused by atmospheric and ionospheric phase-path effects.

It must be pointed out that the phase changes due to the atmosphere amount to about 30 cycles (wavelengths), and those due to the ionosphere about 10 cycles. These changes are obtained by subtracting from the total radio frequency phase change of about 3×10^{11} cycles during the time period of the experiment all the predictable phase-shift caused by the motion of the spacecraft, motion of the stations on the Earth, reference phase changes, light-transit time effects, the effects of the Earth's troposphere, and others. Thus it is implied that the total phase change due to all causes other than the atmosphere and ionosphere of Mars must be known to an accuracy of less than 1 part in 10^{11}.

Before discussing the data obtained in this manner, the geometry of occultation for both entry and exit will be described. At entry into occultation, the spacecraft was at a distance of 25,570 km from the limb of Mars, traveling at a velocity of 2.07 km/sec normal to the Earth–Mars line. The point of tangency on the surface of Mars was at a latitude of 50.5° South and a longitude of 177° East, corresponding to a point between Electris and Mare Chronium. At the time of exit from occultation, the distance from the limb of Mars had increased to 39,150 km, and the point of tangency was located at about 60° North latitude and 34° West longitude, falling within Mare Acidalium.

III. Data

Doppler and amplitude data were taken both during entry and exit by the NASA/JPL Deep Space Instrumentation Facilities (DSIF) at Goldstone, California, and Tidbinbilla and Woomera in Australia. The Goldstone stations (Echo and Pioneer) took standard tracking data doppler (closed-loop) as well as open-loop records (described elsewhere in this report) of the received signal. The Australian stations took only doppler data. At entry all data were taken while the spacecraft transmitter frequency reference was provided by a frequency standard on the Earth. At exit, a 9-sec portion of the data was received while the spacecraft transmitter frequency reference was provided by an on-board crystal oscillator. In the latter mode, the precision of phase measurements is significantly degraded.

Figure 31 shows the range rate doppler residuals (observed minus predicted phase change in 1 sec) based on data received at the various DSIF stations at entry. The points marked O/L have been obtained from the open-loop records by means of spectral density analysis, and the other points are derived directly from data processed through the JPL orbit determination program. One may observe that the data from the various sources show a high degree of consistency, except for the doppler points at $02^h31^m11^s5$, which are suspect because the time of loss of signal is estimated to be between $02^h31^m11^s2$ and $02^h31^m11^s6$ GMT.

A different presentation is shown in Fig. 32, which represents the total phase change as a function of time, derived from Station 11 (Goldstone–Pioneer) doppler residuals. The maximum effect of the ionosphere appears

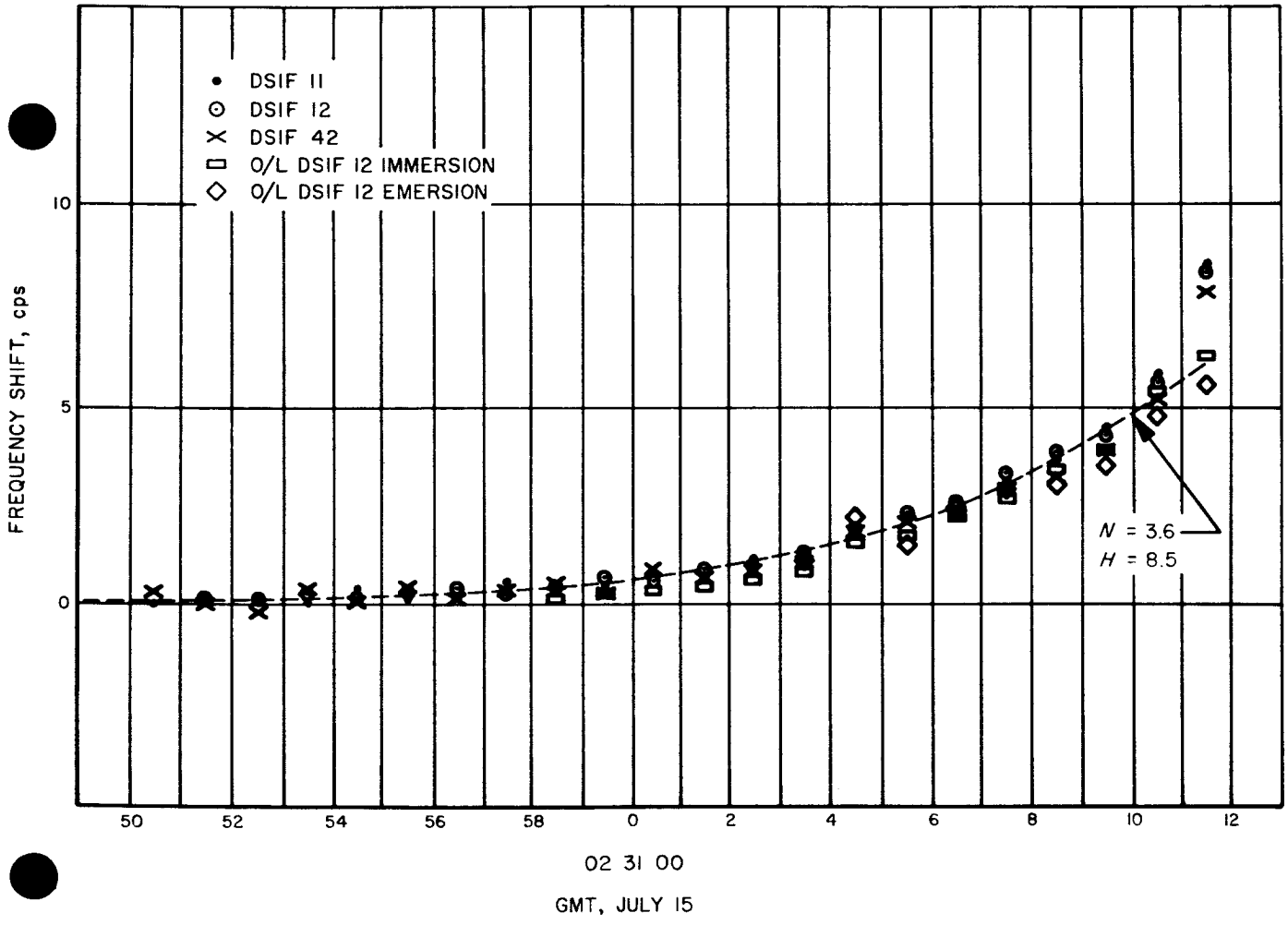

Fig. 31. Range-rate doppler residuals from all DSIF stations

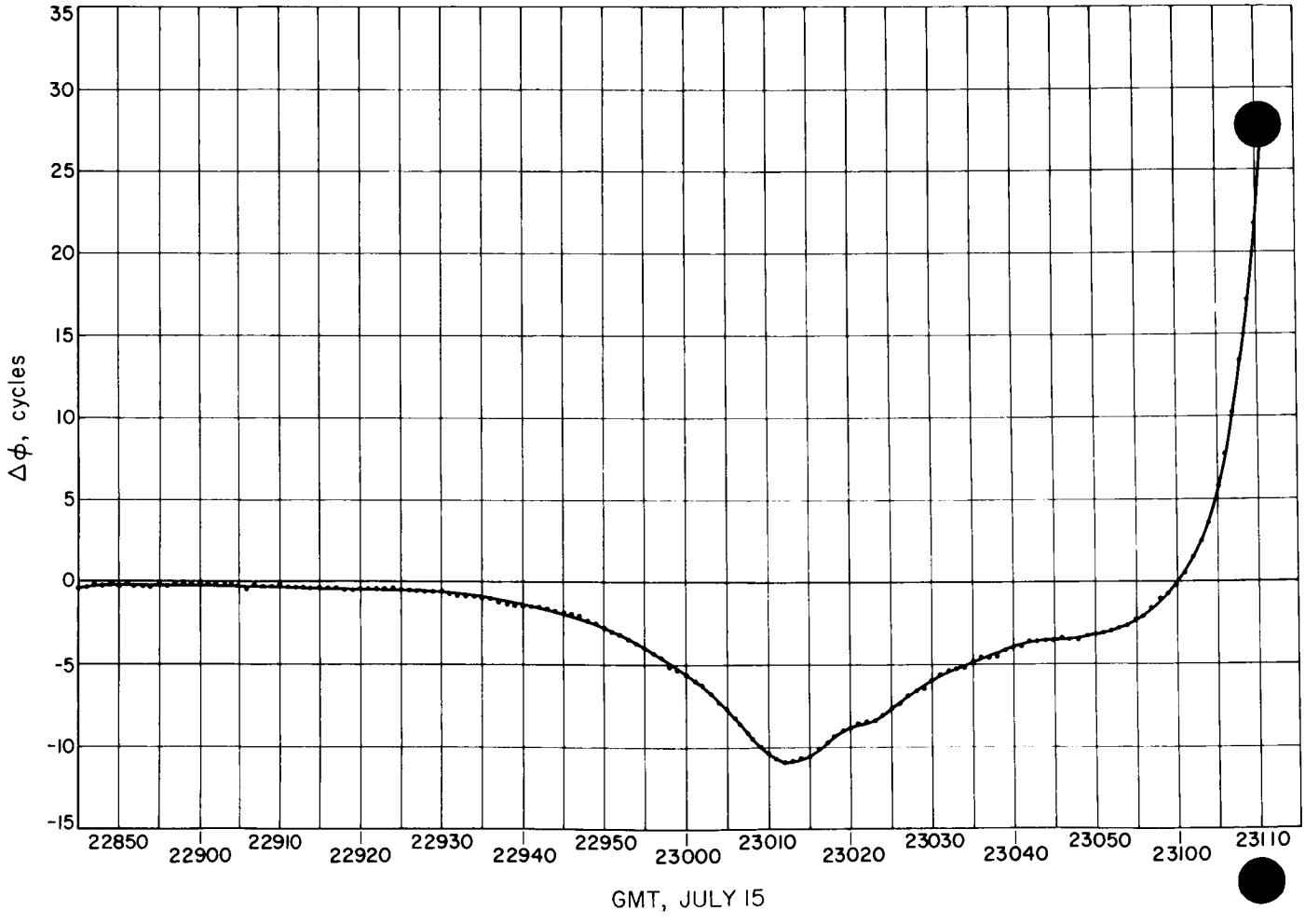

Fig. 32. Phase change at DSIF Station 11

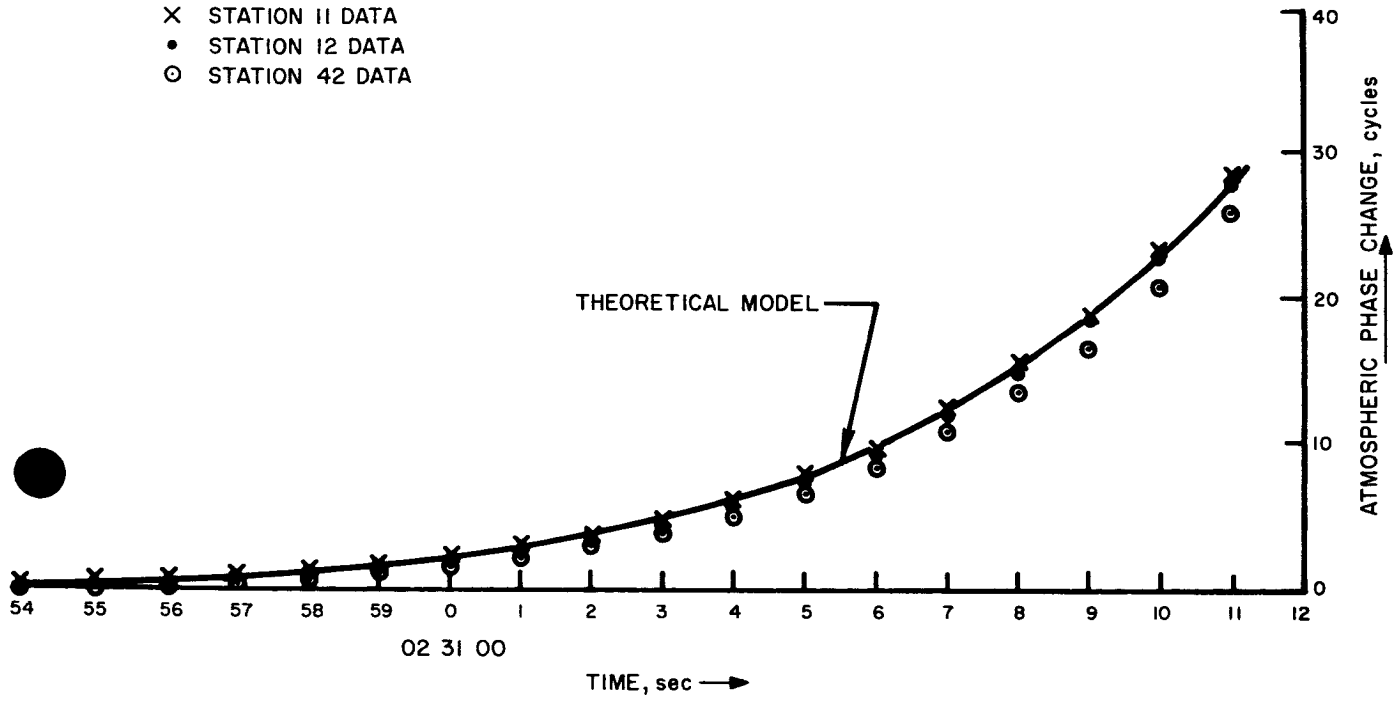

Fig. 33. Phase change due only to atmosphere

at about $02^h30^m10^s$, and the final upswing beginning at about $02^h30^m50^s$ is caused by the neutral atmosphere. It is interesting to note the extreme smoothness of data suggested by the low scatter of the data points.

An expanded portion of the phase change plot is shown in Fig. 33. This graph relates only to the neutral atmosphere, as the estimated effects of the ionosphere have been removed. Signal extinction time is assumed as $02^h31^m11^s2$ GMT.

IV. Atmosphere

The solid curve in Fig. 33 represents the computed phase change for a theoretical exponential model atmosphere having a surface refractivity of 3.7 N-units and a scale height of 9 km. It is obvious that even with this relatively crude model the fit is excellent. The dotted line in Fig. 31 represents the computed doppler residuals for a similar model atmosphere, having a scale height of 8.5 km and $N = 3.6$. As in the case of the phase change, the fit of the data appears to be quite good.

Figure 34, due to G. Fjeldbo of Stanford University, relates maximum phase change, maximum frequency change (doppler), and refractive gain (at the time of extinction of signal of $02^h31^m11^s2$) to the surface refractivity

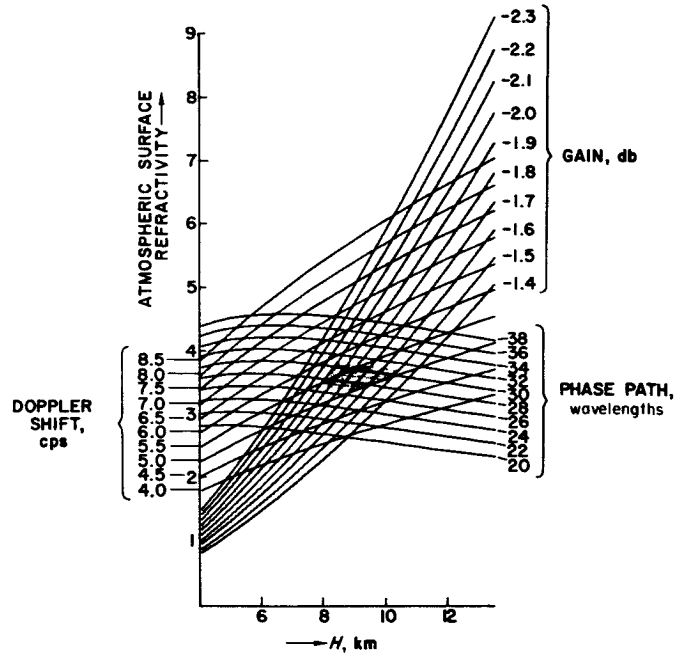

Fig. 34. Maximum changes in doppler shift, phase, and amplitude as functions of surface refractivity and scale height

and scale height of the atmosphere, using an exponential profile of refractivity. Suggested values of 5.5 ±0.5 cps, 29 ±2 cycles, and 1.5 to 2.0 db lead to the stippled area

in the figure. This area corresponds to a surface refractivity of 3.6 ±0.2 *N*-units and a scale height of 9 ±1 km. The gain figure is least reliable, but it can be seen that better values to be obtained from detailed analysis of data from all the stations should help considerably in reducing uncertainty.

A cursory study of the amplitude recordings leads us to believe that signal dropout was due to a diffracting edge, establishing the very important fact that the final ray paths grazed a surface feature on Mars. All references to surface conditions in this paper refer to the altitude of this surface feature. We do not know, of course, its altitude relative to the mean surface of Mars, but the geometry of the experiment would make it likely that it was higher than the mean surface. The refractivity would change by approximately 1% for each 90 m of elevation of the limiting surface feature above the mean surface spheroid of Mars.

In essence then, a simple refractivity model of the Martian atmosphere has been established. It now remains to infer density and pressure, thus bringing into focus the question of composition and temperature.

Figure 35 shows the relationship between refractivity and mass density as a function of composition, ranging from pure CO_2 to 50% CO_2 and 50% argon. To be consistent with the value of scale height determined in this analysis and with the estimated surface temperatures existing at the latitude in question, the composition of the atmosphere must be considered to be predominantly CO_2, with possibly up to 20% argon and small amounts of other gases. This finding is also consistent with the spectroscopically observed CO_2 abundance on Mars.

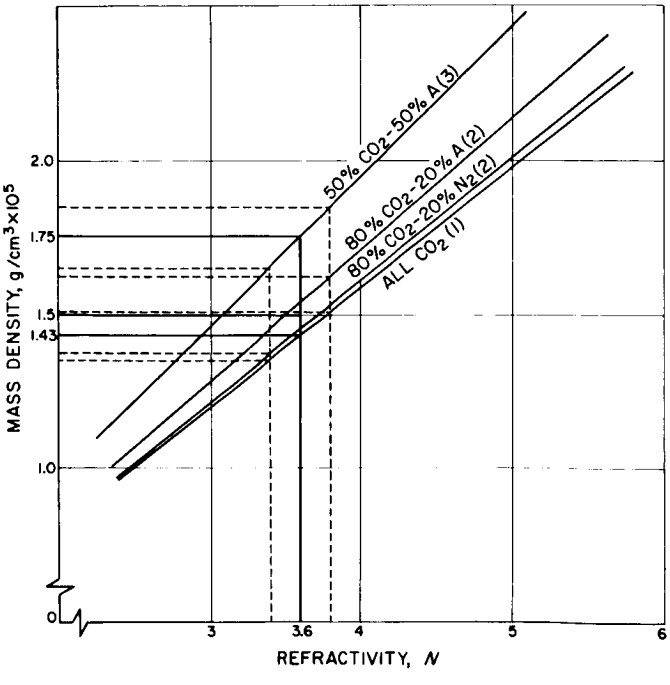

Fig. 35. Mass density vs refractivity for various atmospheric compositions

Two composition models are considered here: (1) pure CO_2 and (2) 80% CO_2 and 20% argon.

For the atmosphere composed of pure CO_2 (model 1) the total number density at the surface corresponding to the measured refractivity values stated above is found to be about 1.9 ±0.1 × 10^{17} molecules/cm³. The mass density (see Fig. 35) is then about 1.43 ±0.10 × 10^{-5} g/cm³. From the measured value of scale height, the temperature range would have to be about 180 ±20°K, leading to a surface pressure range of 4.1 to 5.7 mb.

For the atmosphere consisting of 80% CO_2 and 20% argon (model 2), the various properties are as follows: number density = 2.1 ±0.10 × 10^{17} molecules/cm³; mass density = 1.55 ±0.1 × 10^{-5} g/cm³; temperature = 175 ±20°K; and surface pressure = 4.4 to 6.0 mb.

The number densities derived for these models correspond to from 0.7 to 1.0% of the molecular number density of the Earth's atmosphere at the surface. Since the scale height in the Martian atmosphere is almost equal to that of the Earth, the total number of molecules above a unit area on the surface of Mars is on the order of 1% of that on the Earth.

In addition to the analysis described above, a least-squares fit to the tracking data is being carried out, using a digital computer program due to D. L. Cain, which computes refractive effects in the tracking signal, starting with the orbits of the Earth, Mars, and the spacecraft, and then compares these effects with observations.

Results of a preliminary 5-parameter fit, fitting two atmospheric parameters (surface refractivity and scale height) and three parameters of a single Chapman-layer ionosphere, indicate a surface refractivity of about 3.88 and a scale height of 9.4 km.

The higher value of surface refractivity obtained in this manner could possibly be explained by the circumstance that the exact paths of the up-link and down-link

signals are computed in the program, whereas in the previously described determination these paths were assumed to coincide.

V. Instrumentation

The results described in previous sections have been derived from frequency, phase, and amplitude measurements at the DSIF receiving stations during the occultation experiment. To better understand these measurements, it will be helpful to have a brief description of the DSIF radio system, including the special modifications for the experiment. The block diagram of the system is illustrated in Fig. 36.

The ground station uses a rubidium standard to drive a frequency synthesizer. Its output is then modulated, multiplied 96 times in frequency, amplified, and transmitted to the spacecraft at 2.1 Gc/sec. When the spacecraft receiver is in lock with the ground-station signal, the down-link frequency is derived from the receiver's voltage-controlled oscillator (VCO), which is phase-locked to the received up-link signal. When no up-link is received, however, the down-link frequency is derived from a free-running crystal oscillator in the spacecraft. The RF signal is amplified and transmitted from a high-gain spacecraft antenna.

The ground transmitter and receiver system employs an 85-ft parabolic antenna with a Cassegrainian simultaneous-lobing feed. A traveling-wave maser cooled by a closed-cycle helium refrigerator operating at 4.2°K is used for the receiver front end. After amplification by the maser, the signal is split into two separate receiver channels. The first channel consists of a triple-conversion phase-locked receiver. It is operated in the standard DSIF receiver configuration. This receiver's VCO is kept in phase synchronism with the received signal. By a series of frequency multiplications, divisions, and additions, the transmitter exciter frequency is coherently compared with the receiver VCO to obtain the two-way doppler frequency. The receiver automatic gain control (AGC), which is a received-signal power-level tracking servo, is used to determine received power level. Appropriate AGC voltages were recorded on magnetic tape, and the doppler count was digitized. This system yielded

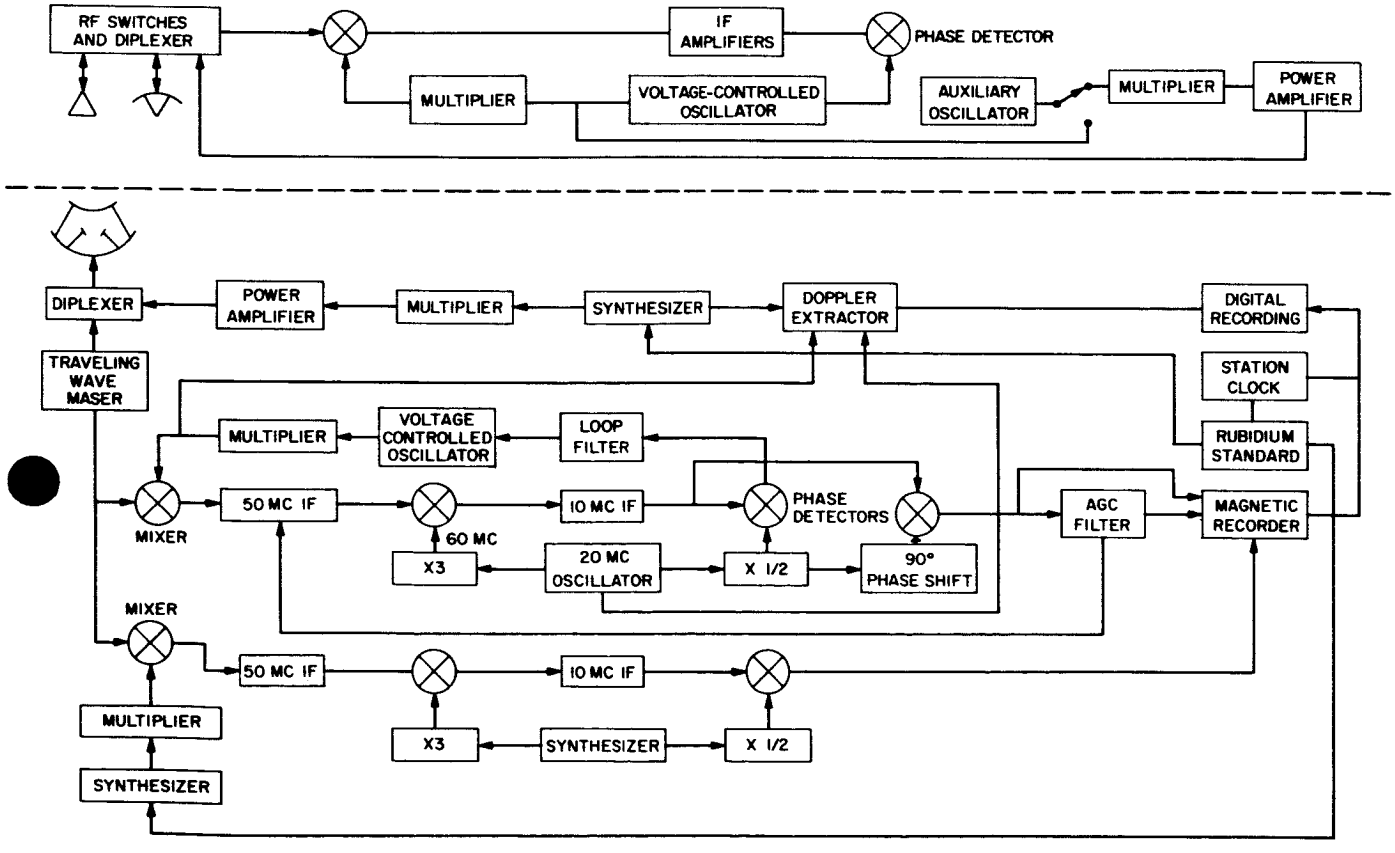

Fig. 36. DSIF instrumentation for the occultation experiment

frequency information in real time. This channel is also used as the sum channel of the pointing system for the simultaneous-lobing antenna.

The second receiver channel, as modified by G. S. Levy, is a manually tuned, constant-gain, triple-conversion superheterodyne operated in a nonstandard configuration. It amplifies and frequency-translates the down-link signal to the audio-frequency region of the spectrum and then records it on magnetic tape. The local-oscillator (LO) signals for this receiver were derived from the rubidium frequency standard, which drives a pair of synthesizers. The first LO frequency was periodically stepped to keep the signal in the receiver's passband. The second and third LO's were derived from the second synthesizer operating at 19.996 Mc/sec. The output of

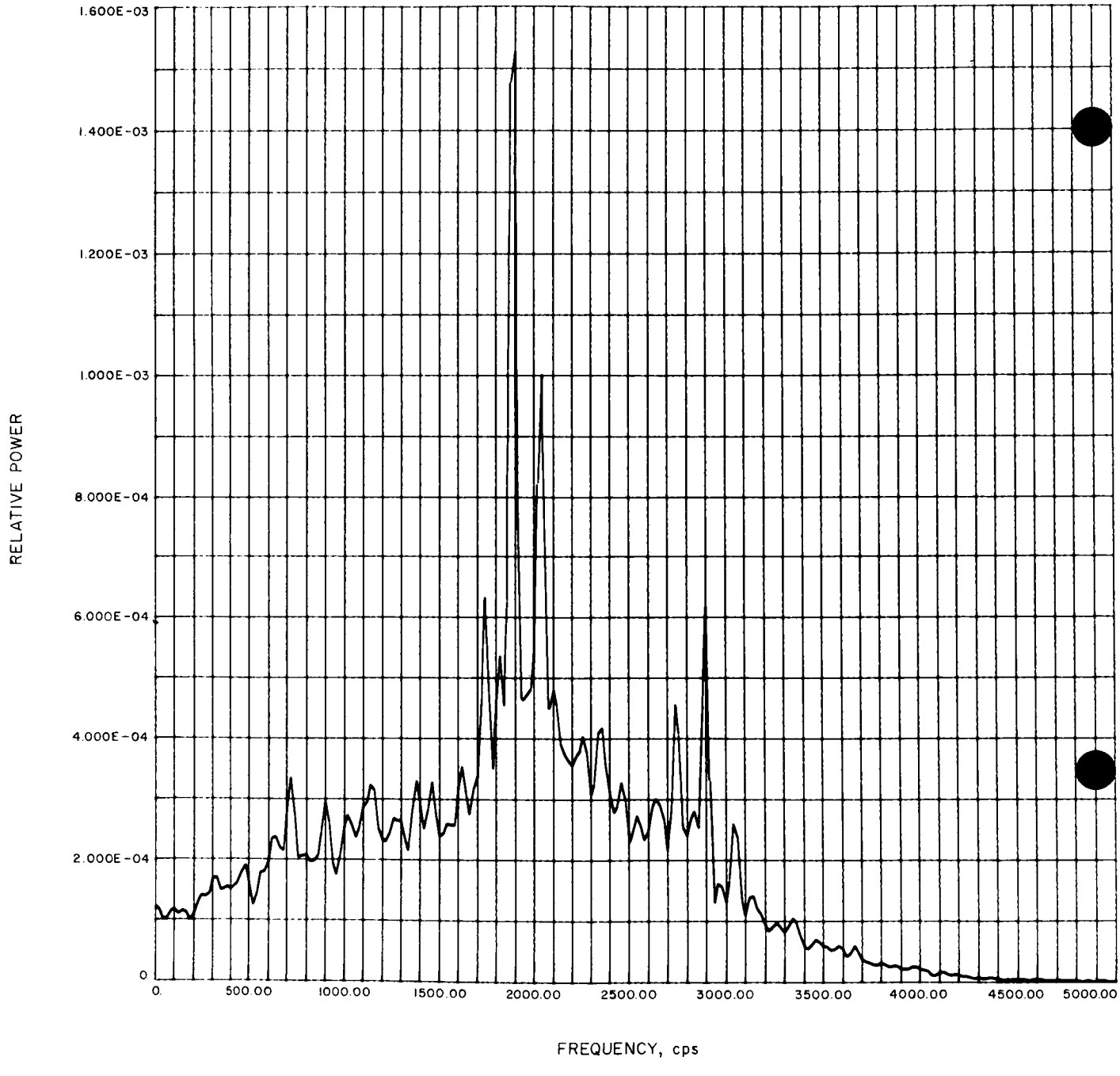

Fig. 37. Power spectrum of signal at the time of switching from one-way to two-way frequency

the third mixer had a passband of 1–3 kc/sec, which was recorded on magnetic tape. Since the LO frequencies were derived from the rubidium standard, the frequency integrity of the doppler was maintained. The analog information on the magnetic tape was digitized after the mission for use in a digital computer.

Figure 37 is a power spectrum of the audio open-loop signal made from the digitized tape on an IBM 7094 computer. The time interval from 03:25:16 to 03:25:17 was chosen. During this second, the one-way frequency, which was first observed as the vehicle reappeared at 03:25:08, was switched off. (This signal component can be seen at 2900 cps.) After the one-way signal decayed, the two-way signal was recorded at an audio frequency of 1900 cps. The phase modulation sidebands at ±150 cps can be seen on both signals.

VI. Conclusions

In conclusion, the results of the preliminary analysis of occultation atmospheric data are summarized in Table 9.

It should be pointed out again that these numbers are the results of less than one month's analysis using relatively crude techniques. As the analysis proceeds, the results will be refined, taking into account additional data as well as more sophisticated theoretical investigations of the physical characteristics of the atmosphere.

Table 9. Preliminary analysis of occultation data

Property	Value
Surface refractivity, N-units	3.6 ±0.2
Scale height, km	8–10
Surface number density, mol/cm³	
All CO_2	$1.9 \pm 0.1 \times 10^{17}$
20% argon	$2.1 \pm 0.10 \times 10^{17}$
Surface mass density, g/cm³	
All CO_2	$1.43 \pm 0.1 \times 10^{-5}$
20% argon	$1.55 \pm 0.10 \times 10^{-5}$
Temperature, °K	
All CO_2	180 ±20
20% argon	175 ±20
Surface pressure, mb	
All CO_2	4.1–5.7
20% argon	4.4–6.0

Acknowledgment

The authors wish to thank the *Mariner* Project and Deep Space Net personnel of JPL for their excellent performance in the preparation for the experiment and the acquisition of data. Special gratitude is due P. K. Eckman and T. W. Hamilton of JPL and B. B. Lusiguan of Stanford University for their many contributions to the success of the experiment.

This paper presents the results of one phase of research carried out at the Jet Propulsion Laboratory, California Institute of Technology, sponsored by the National Aeronautics and Space Administration under Contract No. NAS 7-100, and at Stanford University under National Aeronautics and Space Administration Contracts NSG-377 and NGR 05-020-65.

REFERENCES

1. Kliore, A. J., Cain, D. L., Levy, G. S., Eshleman, V. R., Fjeldbo, G., and Drake, F. D., 1965, *Science*, Vol. 149, p. 1243.
2. Kliore, A. J., Cain, D. L., Levy, G. S., Eshleman, V. R., Drake, F. D., and Fjeldbo, G., 1965, *Astronautics & Aeronautics*, Vol. 7, p. 72.
3. Kaplan, L. D., Münch, G., and Spinrad, H., 1964, *Astrophys. J.*, Vol. 139.
4. Kuiper, G. P., 1964, *Communications of the Lunar and Planetary Laboratory*, University of Arizona, Vol. 2.

REFERENCES (Cont'd)

5. Kliore, A., Cain, D. L., and Hamilton, T. W., 1964, *Technical Report No. 32-674*, Jet Propulsion Laboratory, Pasadena, California.

6. Fjeldbo, G., 1964, *Final Report NSF G 21543, SU-SEL-64-025*, Stanford University.

7. Fjeldbo, G., and Eshleman, V. R., 1965, *J. Geophys. Res.*, Vol. 70, p. 13.